Band structure and charge carrier dynamics in (W,N)-codoped TiO_2 resolved by electrochemical impedance spectroscopy combined with UV–vis and EPR spectroscopies

A. Folli [a], J.Z. Bloh [b], D.E. Macphee [c]

[a] School of Chemistry, Cardiff University, Main Building, Park Place, CF10 3AT Cardiff, Wales, UK
[b] Dechema Research Institute, Theodor-Heuss-Allee 25, 60486 Frankfurt am Main, Germany
[c] Department of Chemistry, University of Aberdeen, Meston Building, Meston Walk, AB24 3UE Aberdeen, Scotland, UK

article info

Keywords:
Mott–Schottky
Photocatalysis
Semiconductor
Paramagnetic
Visible light
Redox potential

abstract

Semiconductor photocatalysis is on the verge of (probably) its most important deployment and boost since the pioneering paper of Fujishima and Honda in 1972. Photo-generation of unbound excitons, i.e. separated conduc-tion band electrons and valence band positive holes, is the fundamental primary process triggering charge separation in solid semiconductors necessary to initiate their photocatalytic activity. Immediately after being generated, charge carriers can undergo processes like recombination, trapping in mid-band-gap states or, paramount for photocatalytic processes, transfer to species adsorbed on the solid semiconductor surface. In TiO_2 and doped TiO_2, interfacial charge transfers are the slowest amongst the primary processes; therefore, electron (and hole) transfer most likely occurs from single electron traps (i.e. involving radical species). We report here on an effective approach combining electrochemical impedance spectroscopy with other spectro-scopic techniques such as UV–vis and electron paramagnetic resonance. This approach allows deriving important information about band structure and following electron dynamics triggered by photon absorption. The redox potentials of the band edges and the influence of the dopants on the band structure are elucidated by electro-chemical impedance spectroscopy combined with UV–vis spectroscopy. Electron dynamics are then studied using electron paramagnetic resonance spectroscopy, to elucidate the photochemical reactions at the basis of the photo-generated electron–hole pairs, and subsequent trapping and/or recombination. Results of a TiO_2 sam-ple containing W and N as dopants (0.1 at.% of W) highlight a narrowing of the intrinsic band gap of about 0.12 eV. The semiconductor visible light photochemistry is driven by diamagnetic donor states $[N_iO]$, and $[N_iO]w$ (formally NO^3), from which electrons can be excited to the conduction band, generating EPR active para-magnetic $[N_iO]^{\bullet}$ and $[N_iO]^{\bullet}_w$ states (formally NO^2). The formation of W^{5+} electron trapping states, energetically more favourable than Ti^{3+} electron trapping states, is also identified.

1. Introduction

Nitrogen doped TiO_2 is one of the most studied visible light photocatalysts. It was first reported by Sato in 1986 as NOx doped tita-nia [1] and in most cases it has shown improved visible light harvesting when compared to ordinary TiO_2 [1–11]. Despite the in-depth under-standing regarding its photoactivity, major drawbacks are yet to be overcome. Charge compensation demands either an increase in oxygen vacancies or decrease in charge carrier (i.e. electrons given the intrinsic n-type character of TiO_2) density upon introduction of the p-dopant (i.e. N), which in turn reduces the overall efficiency of the catalyst [7,12]. Furthermore, Zhao et al. [13] showed that N doped TiO_2 could be sensi-tive to high temperatures and that the maximum amount of nitrogen introduced into titania lattices is quite limited. In recent years, p–n codoping with anion and cation pairs has been proposed in order to offer charge compensation opportunities that minimise crystallographic defects [14–17]. One of the most promising semiconductor amongst the p–n codoped titanias is W(n-type dopant), N(p-type dopant) codoped anatase TiO_2. Improved photonic efficiencies and selectivity for various semiconductor-sensitised photoreactions have been reported [18–20]. Despite such experimental evidence, a clear and complete picture of the fundamental mechanisms for their photoactivity is far from being understood. A significant lack of detailed microscopic information about the effect of the codoping on the structure and electronic proper-ties of TiO_2 has yet to be filled. A few attempts to resolve crystal and band structures through computational studies exist [21,17], however these simulations are not representative of all the possible structures. For example, computed band structures and density of states often refer to substitutional N and substitutional W, however in many cases

Corresponding author.
E-mail address: follia@cardiff.ac.uk (A. Folli).

interstitial N predominates over the substitutional, making calculations and simulations more complex and highly demanding from a computa-tional point of view. We attempt here to provide an experimental approach to this problem. Specifically, we adopt a combination of electrochemical impedance spectroscopy, UV–vis spectroscopy and electron paramagnetic resonance spectroscopy to measure redox potentials of band edges and intraband gap states, optical band gaps and characterise the photochemistry (including exciton formation and trapping under visible-light illumination) of a (W,N) codoped TiO_2 semi-conductor, with the final goal of elucidating a structure-photochemistry relationship.

2. Experimental

(W,N)-codoped TiO_2 containing 0.1 at.% of W was synthesised using a sol–gel route as described in details in one of our previous papers [22]. Mineralogy and crystallinity were interrogated by X-ray diffraction (XRD). XRD patterns were obtained using a Bruker D8 Advance diffractometer equipped to deliver CuK1 X-ray radiation (1.54 Å) at room temperature. Optical absorption investigation was conducted using a modular UV–vis diffuse reflectance spectrometer StellarNet EPP2000. Spectra were processed according to the Kubelka–Munk transform/Tauc plot approach for indirect semiconductors in order to derive information about optical band gaps.

Electrochemical impedance spectroscopy (EIS) measurements were performed using a three-electrode cell consisting of: the (W,N)-codoped TiO_2 sample coated onto a FTO glass slide as a working electrode, a coiled platinum wire counter electrode, and an Ag/AgCl reference electrode (3 mol/L NaCl, + 205 mV vs SHE). The electrodes were fixed in the measurement cell in a way that only the coated part of the FTO glass (circular contact area of 1.77 cm^2) was in contact with the 0.1 mol/L H_2SO_4 electrolyte (more details about the preparation of the coated FTO slides can be found on [33]). Impedance spectra were collected with the use of a Zahner IM6e potentiostat in the potential range of 1.30 V to 0.0 V vs SHE with 25 mV steps. Each spectrum (i.e. at a fixed potential) was recorded in a frequency range of 1×10^5 Hz to 1×10^{-1} Hz with 11 steps per decade and an amplitude of 10 mV. The spectra were subsequently fitted to a Randles circuit (used as an equivalent circuit to represent a simple electrode/electrolyte interface, insets in Fig. 3) to derive the values for the space charge layer capaci-tance (C_{SC}). In the equivalent circuit, a constant phase element (CPE) replaces the ordinary double layer capacitance (C_{SC}) to simulate an uneven surface of the material. The exponential parameter of the CPE was found to be between 0.95 and 1.00, indicating almost ideal capacitance behaviour. Consequently, the space charge layer capacitance was assumed equal to the pseudocapacitance of the CPE. A Mott–Schottky plot was then constructed for each semiconductor oxide by plotting the inversed square of the space charge layer capacitance normalised for the contact area against the potential at which the (C_{SC}) was derived.

EPR spectra were recorded with a JEOL JES-FA200 spectrometer operating either at 77 K with liquid N_2 or at 4 K with liquid He. Before each measurement, the samples were evacuated at room temperature and under high vacuum, ca. 10^{-6} bar. Spectra were recorded in darkness and under in situ irradiation (in the spectrometer cavity) with an Oriel 500 W Xe arc light source, filtered using a 550 nm band-pass filter (Andover Corporation, 550FS80-50 (Q097-05)).

3. Results and discussion

Fig. 1 shows the X-ray diffraction pattern of the (W,N)-codoped TiO_2 containing 0.1 at.% of W together with the pattern of a pure anatase; no crystalline phases other than anatase were detectable in the doped sample. Diffuse reflectance UV–vis spectra of the N- and W-codoped samples (Fig. 2a) are typical of anatase but with an additional feature emphasised in the Tauc plots (Fig. 2b) for the codoped samples, corre-sponding to an energy gap (extrinsic band gap) of 2.32 eV ± 0.02 eV

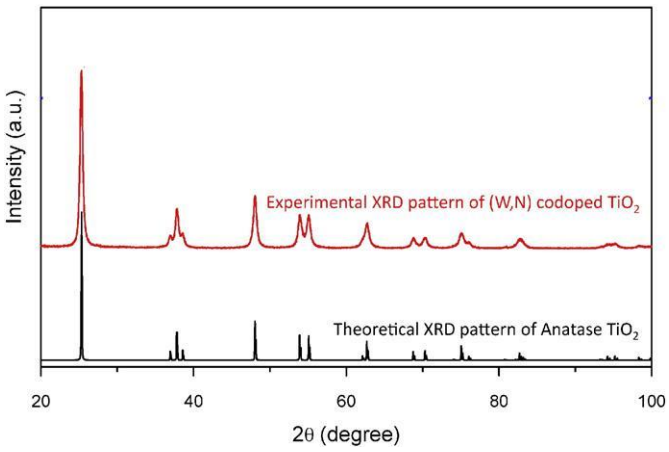

Fig. 1. XRD pattern of (W,N)-codoped TiO_2. The theoretical XRD pattern of anatase TiO_2 is reported as a reference.

and likely to be associated with an electronic transition from an intra-band-gap state due to the presence of N doping [22,9] to the conduction band. This transition is responsible for the observed pale yellow colour

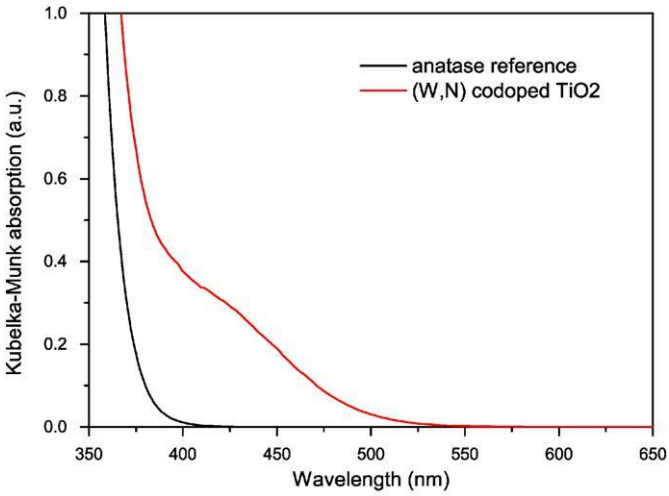

(a) Optical absorption.

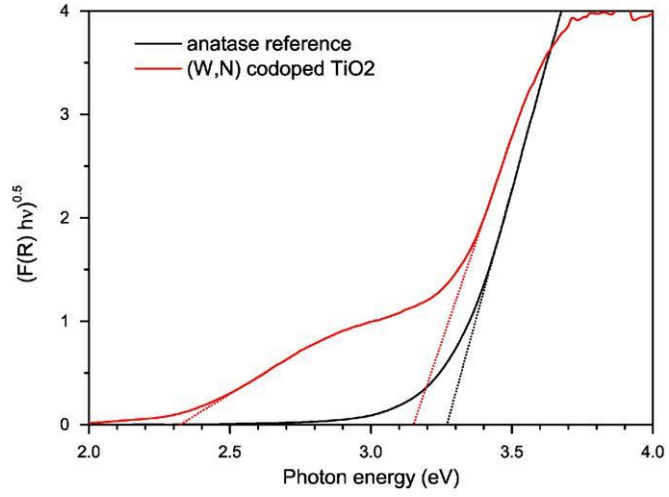

(b) Tauc plot.

Fig. 2. Optical absorption spectrum and Tauc plot of (W,N)-codoped TiO_2. The spectrum and Tauc plot of anatase TiO_2 are reported as a reference.

of the material. The measured intrinsic and extrinsic absorption edges are neither corrected for the phonon energy involved with the indirect transition nor for the exciton binding energy. However, in the case of TiO_2 these quantities are on the order of thousandths of an electron-volt [23]. They are smaller than the average error on the measurement being on the order of hundredths of an electron-volt, and can therefore be neglected. After irradiation with broad band light (UV–A + vis) the (W,N)-codoped TiO_2 assumes a blue colour, which intensity is en-hanced if the material is irradiated in the presence of a hole scavenger. This is the result of a new absorption event occurring between 750 nm to 1000 nm and could be associated with the presence of either Ti^{3+} or W^{5+} traps deep in the band gap. With solely UV–vis data, it is not possible to assert either of the reduced metal centres. The nature of the paramagnetic species associated with this absorption event should be interrogated in order to discriminate between the two possi-ble trapping centres. We will elaborate on this point further below in the discussion.

The conduction band edge is derived using electrochemical imped-ance spectroscopy (EIS) measurements. A Mott–Schottky plot is con-structed as reported in Fig. 3 by plotting the inversed square of the space charge layer capacitance normalised for the contact area against the potential at which the C_{SC} is derived. The extrapolation of the linear trend in the Mott–Schottky plot to the x-axis (potential) leads to the quantity $\delta U_{fb} \pm k_B T\rho$ (see Eq. (1)) from which the flat band potential (U_{fb}, also representing the Fermi level since there is no band bending at flat band conditions) for a given semiconductor oxide could be derived [24–26]

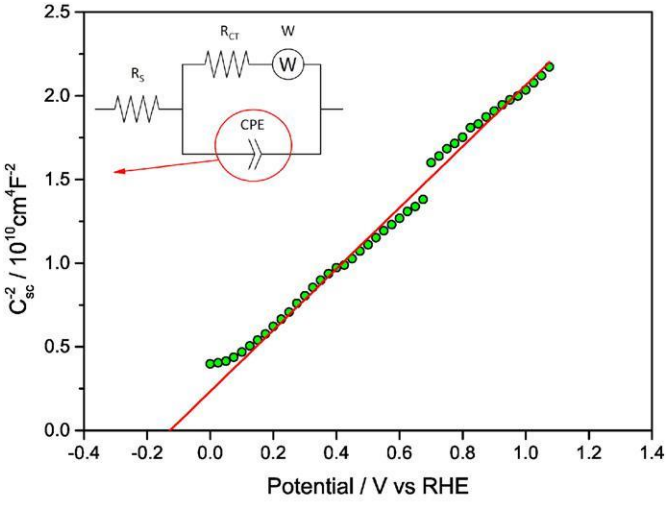

(a) Mott-Schottky replicate 1.

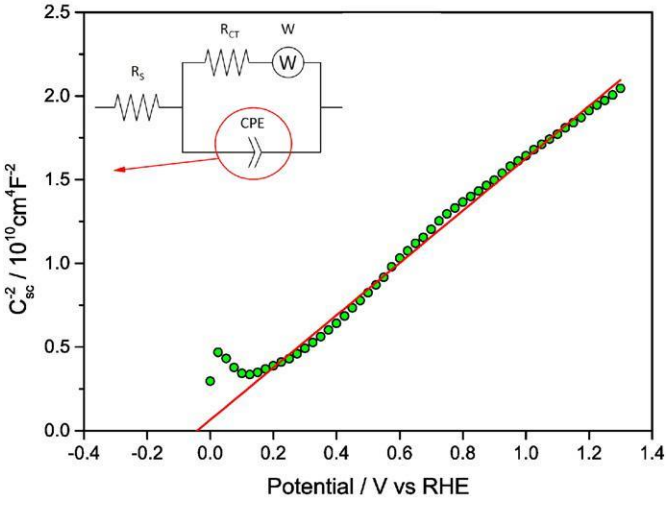

(b) Mott-Schottky replicate 2.

Fig. 3. Mott–Schottky plots of (W,N)-codoped TiO_2. The individual data points are extrap-olated to the x-axis using linear regression (red line). a and b are two replicates of the same sample, then averaged.

$$\delta C_{sc}\rho^{-2} = \frac{2}{\epsilon\,\epsilon_0\,e\,n_d}\left(U - U_{fb} - \frac{k_B T}{e}\right) \quad (1)$$

Additionally, the donor density n_d is calculated from the slope of the linear part using a value of 41 for the dielectric constant of anatase [27]. As the donor density was found higher ($\geq 1 \times 10^{20}$ cm^{-3}) than the effective density of states in the conduction band (2.42×10^{19} cm^{-3}) assuming a value of $1.0 m_e$ for the electron effective mass [28,29], the energy difference between Fermi level and conduction band edge is very small ($\delta k_B T \approx 25$ mV) and they can be assumed to be approximate-ly the same ($U_{cb} \approx U_{fb}$) and equal to −0.06 V ± 0.03 V vs RHE (average of the two Mott–Schottky plots in Fig. 3), defining the positions of the valence band edge and intra-band-gap edge at + 3.09 V ± 0.06 V and + 2.26 V ± 0.05 V respectively (see intrinsic and extrinsic band gaps above). A schematic diagram of the band structure is given in Fig. 4-a.

The lower part of Fig. 4b shows the EPR spectra measured at 77 K in the region of the free electron. The EPR signal recorded can be described as a combination of three different EPR active centres, all associated to N-based species (Fig. 5) [22]. A first paramagnetic centre, b1, can be at-tributed to adsorbed molecular NO [10,4] often detected in the cavities of sol–gel N–TiO_2 [4]. This species exhibits an anisotropic g tensor with rhombic symmetry, $g_{xx} \neq g_{yy} \neq g_{zz}$. The coupling of the unpaired electron with $^{14}_{7}N$ (nuclear spin I = 1; signal multiplicity 2I + 1 = 3) develops a hyperfine structure characterised by 3 × 3 lines. g and A tensors are:

$$g = \begin{bmatrix} 2.003 & & \\ & 2.003 & \\ & & 1.927 \end{bmatrix} \qquad A^{14}N = \begin{bmatrix} 32.0 & & \\ & 31.0 & \\ & & 29.6 \end{bmatrix} \text{ Gauss}$$

A second paramagnetic centre, b2, consists of an interstitial N chem-ically bound to a lattice O ion forming a $[N_iO]^{\bullet}$ [30] group carrying one electron in the singly occupied molecular orbital (SOMO). $[N_iO]^{\bullet}$ is an intra-band gap NO^2 state also exhibiting an anisotropic g tensor with rhombic symmetry [30,4,3,22]:

$$g = \begin{bmatrix} 2.004 & & \\ & 2.005 & \\ & & 2.003 \end{bmatrix} \qquad A\,^{14}N_7 = \begin{bmatrix} 5.6 & & \\ & 2.3 & \\ & & 32.1 \end{bmatrix} \text{ Gauss}$$

A third paramagnetic centre, b3, is present which we showed being generated by a close range interaction of paramagnetic NO^2 with W, $[N_iO]^{\cdot}{}_W$ [22]. The signal is the combination of two contributions; one for the four EPR equivalent isotopomers associated with the W zero nuclear spin nuclides, i.e. $^{180}_{74}W$, $^{182}_{74}W$, $^{184}_{74}W$ and $^{186}_{74}W$ (effectively the same as b2 however distorted due to the surrounding lattice W, Fig. 6a); a second one for the isotopomer associated with $^{183}_{74}W$ that is able to generate super hyperfine splitting as the electron in the NO^2 SOMO couples with the $^{183}_{74}W$ 1/2-spin nucleus (Fig. 6b). The component b3′ without super hyperfine splitting is described by:

$$g = \begin{bmatrix} 2.001 & & \\ & 2.002 & \\ & & 2.000 \end{bmatrix} \qquad A\,^{14}N_7 = \begin{bmatrix} 8.0 & & \\ & 8.0 & \\ & & 50.0 \end{bmatrix} \text{ Gauss}$$

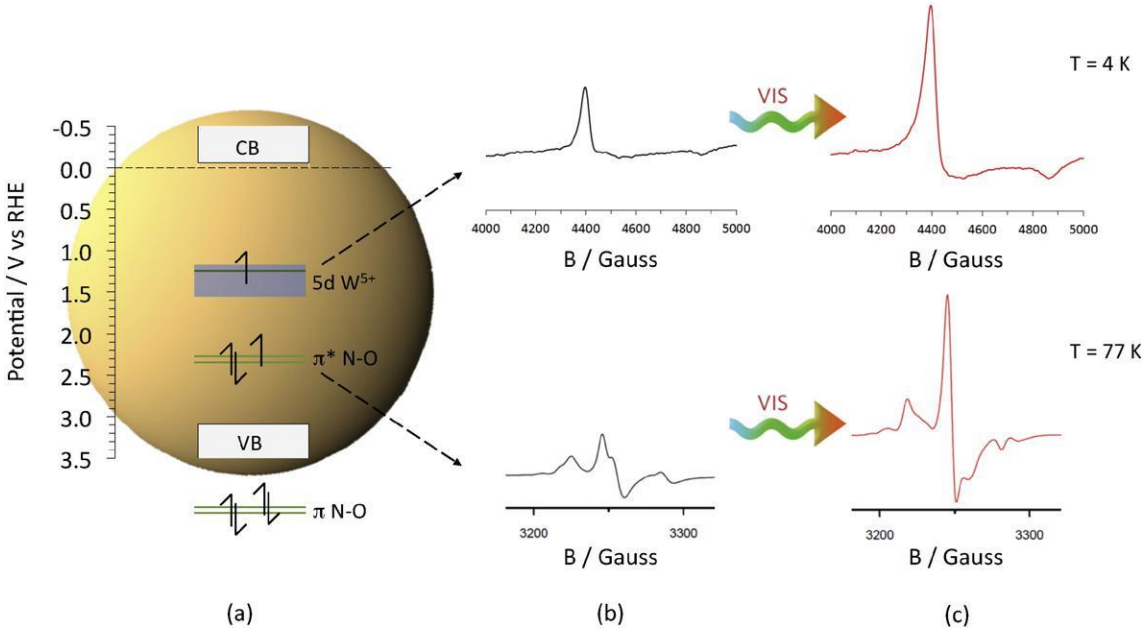

Fig. 4. (a) Band structure diagram of (W,N)-codoped TiO_2 containing 0.1 at.% of W. (b) CW X-band Electron Paramagnetic Resonance spectra before in-situ irradiation with 550 nm wave-length light and (c) CW X-band Electron Paramagnetic Resonance spectra after in-situ irradiation with 550 nm wavelength light. EPR signals related to the N-based species and W-based species were recorded at different ranges of magnetic field (due to the very distincted g-values) and at different temperature, i.e. 77 K for the N-based species and 4 K for W^{5+}. The much lower temperature necessary for detecting W^{5+} with EPR is due to the too short relaxation time at 77 K.

whilst the component of b3″ with super hyperfine splitting (accounting for 14.31%, i.e. the abundance of $_{74}{}^{183}W$), by:

g 2 2:001 3 A 14 N 7 2 8:0 3 Gauss A 183 W 74 2 b1:0 3 Gauss :
2:002 8:0 16:0
¼ 7 ¼ ½ & 74 ¼ ½ &
4 2:000 5 4 50:0 5 4 22:0 5

In this region, there seems to be no evidence for the presence of Ti^{3+}, that – if present in the semiconductor oxide – should be visible at 77 K in this range of magnetic field [31]. On the contrary when the temperature is lowered to 4 K in liquid He, a new anisotropic g tensor with axial symmetry, $g_\perp \neq g_\parallel$, appears at higher magnetic fields (upper part of Fig. 4b), which components are:

g ¼ 1:477 :
1:342

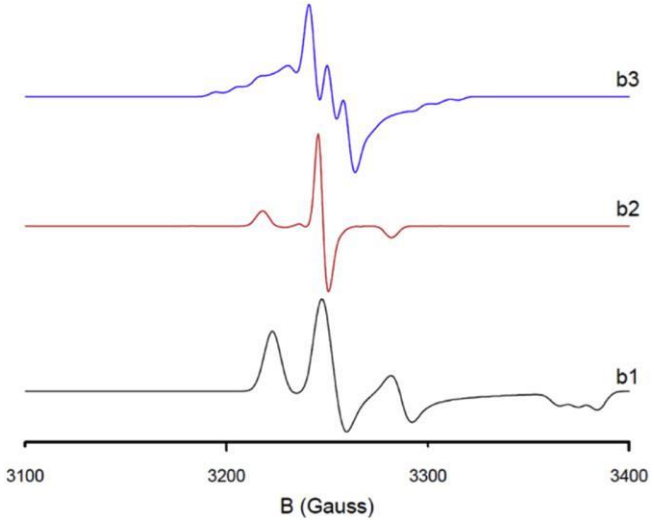

Fig. 5. Simulated single spectra of the three EPR active centres b1, b2 and b3. b1 corre-sponds to an adsorbed molecular paramagnetic NO; b2 corresponds to an interstitial N chemically bound to a lattice O ion forming a [NiO] group carrying one electron in the sin-gly occupied molecular orbital (SOMO); b3 is a the species chemically equivalent to b2 but influenced by a short-range interaction with W. The intensities in this figure are relative to the components alone. The combination (with different relative contributions) of the spectra b1, b2, and b3 make up for the overall spectra on the lower parts of Fig. 4-b and c [22].

The position of this signal is in agreement with a similar signal previously recorded by Zhao et al. [32] for W^{5+} in WO_3/TiO_2 mixed oxide system. g components of octahedral W^{5+} are significantly lower than the ones of isoelectronic d1 ions like Mo^{5+} or V^{4+}. This is due to a greater spin-orbit coupling for tungsten [34]. The presence of W^{5+} before illumination can be explained through charge compensation mechanisms. W^{6+} is replacing Ti^{4+} ions in the TiO_2 lattice. The excess of positive charges clearly needs to be compensated by corresponding negative ones. There are three possible mechanisms for compensating the extra positive charges carried by W^{6+}: ionic, electronic and comple-mentary doping, Eqs. (2)–(4) respectively.

$$2\,WO_3 \xrightarrow{3\ TiO} {}^{2}\,2\,W_{Ti}^{\bullet\bullet} + V_{Ti}^{00\ 00} + 6\,O_O^{x} \quad (2)$$

$$WO \xrightarrow{TiO_2} W^{\bullet\bullet} + 2O^{x} + 2e^{0} \quad \frac{1}{3}\,O$$

$$3\,Ti + O + 2 \quad (3)$$

$$WO_3 + O_2 + 2NH_3 \rightarrow W_{Ti}^{\bullet\bullet} + 2\,½NO\&O^{0} + 3\,H_2O \quad (4)$$

All the three mechanisms can be simultaneously present (albeit for low W doping the compensation with N seems to be the favourite one [33]). The electronic charge compensation (i.e. formation of free elec-trons, Eq. (3)) would lead to a noticeable increase in the donor density of the materials. However, electrochemical impedance spectroscopy for this codoped system showed no significant variation in the donor density when compared to undoped anatase TiO_2. A possible interpreta-tion for this is that if charge compensating electrons are formed, they are trapped in energetically favourable states:

$$Ti_{Ti}^{x} + e^{0} \rightarrow Ti_{Ti}^{0} \quad (5)$$

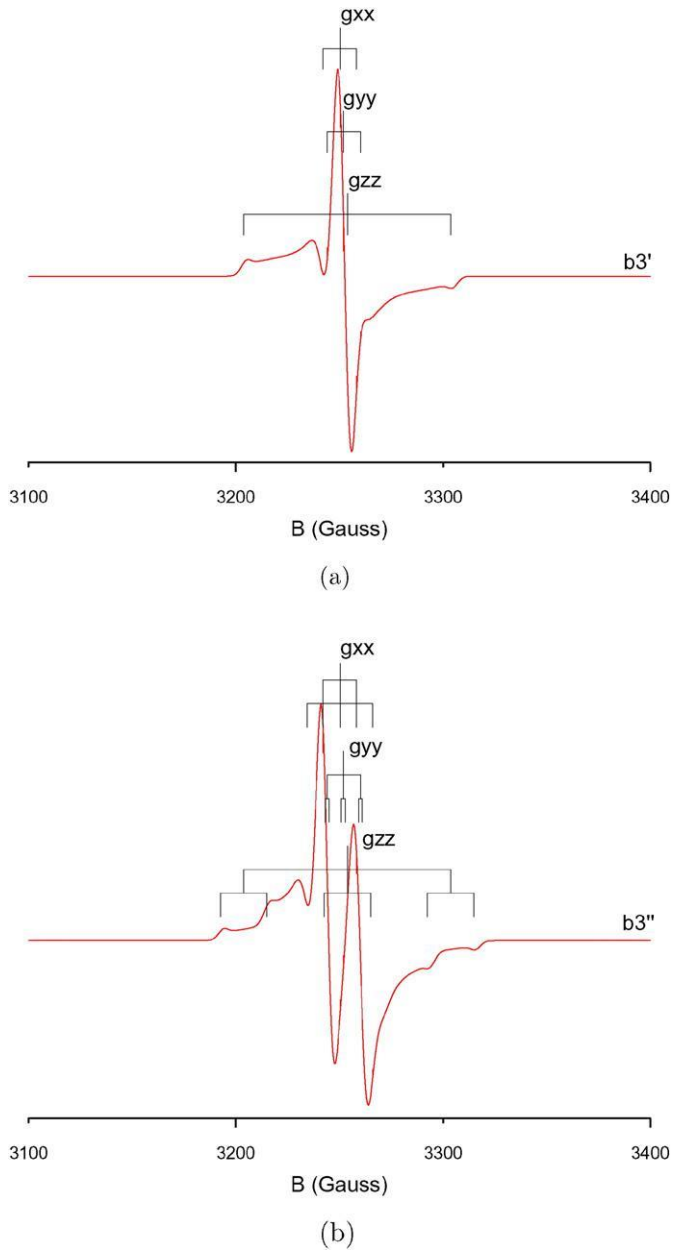

Fig. 6. Simulated single EPR profiles of: (a)-b3′ four equivalent ½N_i O&$_x$W paramagnetic isotopomers carrying a null spin ^{x}W nuclide, x = 180, 182, 184, 186; (b)-b3″ ½N_iO&$_{183\_w}$ paramagnetic isotopomer carrying ^{183}W nuclide, I = 1/2.

$$W_{Ti} + e^{0} \rightarrow W_{Ti} : \qquad (6)$$

The absence of Ti^{3+} (Ti_{Ti}^{0} in Kröger–Vink notation) in the EPR spectra but the clear presence of W^{5+} (W_{Ti} in Kröger–Vink notation) would suggest a more energetically favourable (i.e. deeper in the band gap) trapping of the compensating electrons as reduced tungsten.

Having identified the nature of the EPR active species, we can now explain the spectral changes when the sample is irradiated with visible light (550 nm wavelength) (Fig. 4c) which are a consequence of the electron dynamics within the structure of the doped semiconductor. As in the case of N doping only, a large fraction of the nitrogen centres is diamagnetic before light irradiation, carrying two paired electrons in the highest occupied molecular orbital. They can be seen as a $[N_iO]^{-}$, intra-band gap NO^{3} states [9], and similarly, $[N_iO]^{W}$ and intra-band gap NO^{3} states characterised by close range N–W coupling. The dark spectrum is therefore dominated by the signal of adsorbed molec-ular NO [10,4] (b1 centre). Upon irradiation with visible light, electron transitions CB NO^{3} occur, leaving behind a much larger quantity of paramagnetic NO^{2} states that can be easily detected by EPR. The signal of the adsorbed molecular NO does not significantly change but the considerable formation of paramagnetic $[N_iO]^{\bullet}$, and $[N_iO]_W$ centres is responsible for the new profile of the EPR spectrum (lower part of Fig. 4c) together with the increased intensity. After switching the light off (spectrum not reported here), the intensity of the $[N_iO]^{\bullet}$ and $[N_iO]_W$ signals decreases very slowly whilst, once again, the component assigned to the adsorbed molecular NO does not show a significant change. However, even after more than 30 min in the dark, the overall spectrum is still dominated by the $[N_iO]^{\bullet}$ and $[N_iO]_W$ centres and the ini-tial spectrum before irradiation not recovered. As far as W^{5+} signal is concerned (upper part of Fig. 4c), it is evident how the signal intensity increases upon irradiation with visible light. On the basis of this spectral change, it is assumed that the electrons excited from the NO^{3-} states to the conduction band fall into W^{5+} trapping state, effectively reducing more lattice W^{6+} to W^{5+}. The electron trapping process is expected to be maximum under the conditions adopted given in the absence of electron scavengers in the EPR cell. Furthermore, we can now assert with a sufficient degree of confidence that the optical absorption event observed at 750 nm to 1000 nm after light irradiation (hence after quantitative formation of W^{5+} states), should be attributed to CB ← W^{5+} transitions.

4. Conclusions

The coupling of electrochemical impedance spectroscopy with other spectroscopic techniques such as UV–vis and electron paramagnetic resonance proved to be an effective approach to obtain useful information about semiconductor band structure, including band edge and intra-band gap state redox potentials, and follow photon-induced charge carriers dynamics. This approach has been described here using a (W,N) codoped TiO_2 semiconductor as a testing material.

The simultaneous presence of W and N causes a shift in the potential of the conduction band edge; from −0.2 V versus RHE for the undoped anatase TiO_2 to −0.06 V versus RHE, effectively narrowing the intrinsic band gap by about 0.12 eV when compared to the 3.27 eV here measured for the undoped anatase TiO_2.

Upon irradiation with green light (550 nm) paramagnetic intra-band gap species $[N_iO]^{\bullet}$ and $[N_iO]^{W}$ (formally NO^{2}) are photo-generated as a consequence of photon absorption and electronic transi-tions from diamagnetic donor states $[N_iO]^{-}$, and $[N_iO]^{-}_W$ (formally NO^{3}) to the TiO_2 conduction band. The optical transition from the NO^{3} intra-band gap states to the conduction band was measured around 2.32 eV. In the absence of effective electron scavengers, conduction band electrons are preferentially trapped as reduced tungsten, W^{5+}, as experimental evidences show that these trapping states should be located at lower energy than Ti^{3+} traps commonly found in undoped TiO_2 semiconductors.

Acknowledgement

The Authors are grateful to the European Commission for the financial support through the European Project Light^{2}CAT. Light^{2}CAT is funded by the European Union Seventh Framework Programme (FP7) under the grant agreement no. 283062 Eco-Innovation, Theme Environment. The authors also gratefully acknowledge the British Council and FAPESP (São Paulo Research Foundation) for the financial support of the workshop ELSOL — Electrochemical solutions for contem-porary problems.

References

[1] S. Sato, Photocatalytic activity of NOx-doped TiO_2 in the visible light region, Chem. Phys. Lett. 123 (1–2) (1986) 126–128, http://dx.doi.org/10.1016/0009-2614(86)87026-9.

[2] S. Sato, R. Nakamura, S. Abe, Visible-light sensitization of TiO_2 photocatalysts by wet-method N doping, Appl. Catal. A 284 (1–2) (2005) 131–137 (URL http://www.sciencedirect.com/science/article/B6TF5-4FGX5BX-1/2/29f9fde7d951121dc86f03b9943df1ce).

[3] S. Livraghi, K. Elghniji, A.M. Czoska, M.C. Paganini, L.M. Ksibi, Nitrogen-doped and ni-trogen–fluorine-codoped titanium dioxide. Nature and concentration of the photoactive species and their role in determining the photocatalytic activity under visible light, J. Photochem. Photobiol. A 205 (2–3) (2009) 93–97, http://dx.doi.org/10.1016/j.jphotochem.2009.04.010.

[4] S. Livraghi, M.R. Chierotti, E. Giamello, G. Magnacca, M.C. Paganini, G. Cappelletti, C.L. Bianchi, Nitrogen-doped titanium dioxide active in photocatalytic reactions with visible light: a multi-technique characterization of differently prepared materials, J. Phys. Chem. C 112 (44) (2008) 17244–17252, http://dx.doi.org/10. 1021/jp803806s (URL http://www.scopus.com/inward/record.url?eid=2-s2.0-56549093562&partnerID=40&md5=0195d76041450fc3cbd8e1726a750925).

[5] D. Li, H. Haneda, S. Hishita, N. Ohashi, Visible-light-driven NF-codoped TiO_2 photocatalysts. 1. Synthesis by spray pyrolysis and surface characterization, Chem. Mater. 17 (10) (2005) 2588–2595, http://dx.doi.org/10.1021/cm049100k.

[6] A. Kubacka, G. Colón, M. Fernández-García, N- and/or W-(co)doped TiO_2-anatase catalysts: effect of the calcination treatment on photoactivity, Appl. Catal. B Environ. 95 (3–4) (2010) 238–244, http://dx.doi.org/10.1016/j.apcatb.2009.12.028.

[7] H. Irie, Y. Watanabe, K. Hashimoto, Nitrogen-concentration dependence on photo-catalytic activity of TiO_2-xNx powders, J. Phys. Chem. B 107 (23) (2003) 5483–5486, http://dx.doi.org/10.1021/jp030133h.

[8] X. Chen, C. Burda, The electronic origin of the visible-light absorption properties of C-, N- and S-Doped TiO_2 nanomaterials, J. Am. Chem. Soc. 130 (15) (2008) 5018–5019, http://dx.doi.org/10.1021/ja711023z.

[9] G. Barolo, S. Livraghi, M. Chiesa, M.C. Paganini, E. Giamello, Mechanism of the photoactivity under visible light of N-doped titanium dioxide. Charge carriers mi-gration in irradiated N-TiO_2 investigated by electron paramagnetic resonance, J. Phys. Chem. C 116 (39) (2012) 20887–20894, http://dx.doi.org/10.1021/jp306123d.

[10] C. Di Valentin, E. Finazzi, G. Pacchioni, A. Selloni, S. Livraghi, M.C. Paganini, E. Giamello, N-doped TiO2: theory and experiment, Chem. Phys. 339 (13) (2007) 44–56, http://dx.doi.org/10.1016/j.chemphys.2007.07.020 (URL http://www.sciencedirect.com/science/article/pii/S0301010407002893).

[11] C. Di Valentin, G. Pacchioni, A. Selloni, S. Livraghi, E. Giamello, Characterization of paramagnetic species in N-doped TiO_2 powders by EPR spectroscopy and DFT calculations, J. Phys. Chem. B 109 (23) (2005) 11414–11419, http://dx.doi.org/10.1021/jp051756t.

[12] K.-i. Yamanaka, T. Morikawa, SI-charge-carrier dynamics in nitrogen-doped TiO_2 powder studied by femtosecond time-resolved diffuse reflectance spectroscopy, J. Phys. Chem. C 2 (2013) 1–3, http://dx.doi.org/10.1021/jp209210u.

[13] Y. Zhao, X. Qiu, C. Burda, The effects of sintering on the photocatalytic activity of N-doped TiO_2 nanoparticles, Chem. Mater. 20 (8) (2008) 2629–2636, http://dx.doi.org/10.1021/cm703043j.

[14] C.D. Valentin, E. Finazzi, G. Pacchioni, A. Selloni, S. Livraghi, A.M. Czoska, M.C. Paganini, E. Giamello, Density functional theory and electron paramagnetic resonance study on the effect of N F codoping of TiO_2, Chem. Mater. 20 (2008) 3706–3714, http://dx.doi.org/10.1021/cm703636s.

[15] T.M. Breault, B.M. Bartlett, Composition-dependence of TiO_2:(Nb, N)-x compounds on the rate of photocatalytic methylene blue dye degradation SUPPORTING INFORMATION, J. Phys. Chem. C 117 (2013) 1–13.

[16] A.M. Czoska, S. Livraghi, M.C. Paganini, E. Giamello, C. Di Valentin, G. Pacchioni, The nitrogen–boron paramagnetic center in visible light sensitized N–B co-doped TiO_2. Experimental and theoretical characterization, Phys. Chem. Chem. Phys. 13 (1) (2011) 136–143, http://dx.doi.org/10.1039/C0CP00143K.

[17] A.M. Márquez, J.J. Plata, Y. Ortega, J.F. Sanz, G. Colón, A. Kubacka, M. Fernández-García, Making photo-selective TiO_2 materials by cation–anion codoping: from structure and electronic properties to photoactivity, J. Phys. Chem. C 116 (35) (2012) 18759–18767, http://dx.doi.org/10.1021/jp3045143.

[18] A.K.L. Sajjad, S. Shamaila, J. Zhang, Study of new states in visible light active W, N co-doped TiO_2 photo catalyst, Mater. Res. Bull. 47 (11) (2012) 3083–3089, http://dx.doi.org/10.1016/j.materresbull.2012.08.032 (URL http://www.sciencedirect.com/science/article/pii/S0025540812006034).

[19] A. Kubacka, B. Bachiller-Baeza, G. Colon, M. Fernandez-Garcia, W,N-codoped TiO_2-anatase: a sunlight-operated catalyst for efficient and selective aromatic hydrocar-bons photo-oxidation, J. Phys. Chem. C 113 (20) (2009) 8553–8555, http://dx.doi.org/10.1021/jp902618g.

[20] J.Z. Bloh, A. Folli, D.E. Macphee, Photocatalytic NOx abatement: why the selectivity matters, RSC Adv. 4 (86) (2014) 45726–45734, http://dx.doi.org/10.1039/ C4RA07916G (URL http://xlink.rsc.org/?DOI=C4RA07916G).

[21] V. Çelik, E. Mete, Range-separated hybrid exchange-correlation functional analyses of anatase TiO_2 doped with W, N, S, W/N, or W/S, Phys. Rev. B 86 (20) (2012) 205112, http://dx.doi.org/10.1103/PhysRevB.86.205112.

[22] A. Folli, J.Z. Bloh, E.-p. Beukes, R.F. Howe, D.E. Macphee, Photogenerated Charge Carriers and Paramagnetic Species in (W,N)- Codoped TiO2 Photocatalysts under Visible-Light Irradiation: An EPR Study, J. Phys. Chem. C 117 (42) (2013) 22149–22155.

[23] J. Pascual, J. Camassel, H. Mathieu, Fine structure in the intrinsic absorption edge of TiO_2, Phys. Rev. B 18 (10) (1978) 5606–5614.

[24] N.F. Mott, The theory of crystal rectifiers, P. Roy. Soc. London, A Mat. 171 (944) (1939) 27–38.

[25] W. Schottky, Zur Halbleitertheorie der Sperrschicht- und Spitzengleichrichter, Z. Phys. 113 (5–6) (1939) 367–414.

[26] W. Schottky, Vereinfachte und erweiterte Theorie der Randschicht-gleichrichter, Z. Phys. 118 (9–10) (1942) 539–592.

[27] I. Oja, A. Mere, M. Krunks, R. Nisumaa, C.-H. Solterbeck, M. Es-Souni, Structural and electrical characterization of TiO_2 films grown by spray pyrolysis, Thin Solid Films 515 (2) (2006) 674–677, http://dx.doi.org/10.1016/j.tsf.2005.12.243 (URL http://linkinghub.elsevier.com/retrieve/pii/S0040609005025708).

[28] H. Tang, K. Prasad, R. Sanjines, P.E. Schmid, F. Levy, Electrical and optical properties of TiO_2 anatase thin films, J. Appl. Phys. 75 (4) (1994) 2042, http://dx.doi.org/10.1063/1.356306 (URL http://scitation.aip.org/content/aip/journal/jap/75/4/10.1063/1.356306).

[29] B. Enright, D. Fitzmaurice, Spectroscopic determination of electron and hole effec-tive masses in a nanocrystalline semiconductor film, J. Phys. Chem. 100 (1996) 1027–1035.

[30] S. Livraghi, M.C. Paganini, E. Giamello, A. Selloni, C. Di Valentin, G. Pacchioni, Origin of photoactivity of nitrogen-doped titanium dioxide under visible light, J. Am. Chem. Soc. 128 (49) (2006) 15666–15671, http://dx.doi.org/10.1021/ja064164c.

[31] R.F. Howe, M. Gratzel, EPR observation of trapped electrons in colloidal titanium di-oxide, J. Phys. Chem. 89 (21) (1985) 4495–4499, http://dx.doi.org/10.1021/ j100267a018.

[32] D. Zhao, C. Chen, C. Yu, W. Ma, J. Zhao, Photoinduced electron storage in WO_3/TiO_2 nanohybrid material in the presence of oxygen and postirradiated reduction of heavy metal ions, J. Phys. Chem. C 113 (2009) 13160–13165, http://dx.doi.org/10. 1021/jp9002774.

[33] J.Z. Bloh, A. Folli, D.E. Macphee, Adjusting nitrogen doping level in titanium dioxide by codoping with tungsten: properties and band structure of the resulting materials, J. Phys. Chem. C 118 (2014) 21281–21292, http://dx.doi.org/10.1021/jp507264g.

[34] D. Bravo, X. Ruiz, F. Díaz, F. López, EPR of tungsten impurities in $KTiOPO_4$ single crys-tals grown from molten tungstate solutions, Phys. Rev. B 52 (5) (1995) 3159–3169 (URL http://www.ncbi.nlm.nih.gov/pubmed/9981432).